

Stationary time-vertex signal processing

Andreas Loukas* and Nathanaël Perraudin*
École Polytechnique Fédérale Lausanne, Switzerland

May 2016

Abstract

The goal of this paper is to improve learning for multivariate processes whose structure is dependent on some *known* graph topology. Typically, the graph information is incorporated to the learning process via a smoothness assumption postulating that the values supported on well connected vertices exhibit small variations. We argue that smoothness is not enough. To capture the behavior of complex interconnected systems, such as transportation and biological networks, it is important to train expressive models, being able to reproduce a wide range of graph and temporal behaviors.

Motivated by this need, this paper puts forth a novel definition of time-vertex wide-sense stationarity, or *joint stationarity* for short. We believe that the proposed definition is natural, at it elegantly relates to existing definitions of stationarity in the time and vertex domains. We use joint stationarity to regularize learning and to reduce computational complexity in both estimation and recovery tasks. In particular, we show that for any jointly stationary process: (a) one can learn the covariance structure from $\mathcal{O}(1)$ samples, and (b) can solve MMSE recovery problems, such as interpolation, denoising, forecasting, in complexity that is linear to the edges and timesteps. Experiments with three datasets suggest that joint stationarity can yield significant accuracy improvements in the reconstruction effort.

Index terms— stationarity, multivariate time-vertex processes, harmonic analysis, graph signal processing, PSD estimation.

1 Introduction

One of the main challenges when working with multivariate processes is to learn their statistical structure from few samples. Concretely, suppose that we wish to estimate the first two moments of a process $\mathbf{X} \in \mathbb{R}^{N \times T}$, where N is the number of variables and T the number of timesteps. If no restricting assumptions are made (other than the first four moments are finite) then the number of samples needed to attain statistical significance is up to a logarithmic factor proportional to $\mathcal{O}(NT)$, the degrees of freedom [1]. Assuming that the process is time wide-sense stationarity (TWSS) is very helpful as it reduces the degrees of freedom of the system –and thus the sample requirement– by a factor of T . Even a linear dependency on N however is often problematic in practice, when the number of variables is large and the ability to obtain multiple samples limited.

The goal of this paper is to improve learning for the specific cases when the multivariate process is supported on the vertex set and is statistically dependent on the edge set of some known graph topology. Whether examining epidemic spreading [2], how traffic evolves in the roads of a city [3], or neuronal activation patterns present in the brain [4], many of the high-dimensional processes one encounters are inherently constrained by some underlying network. This realization has been the driving force behind recent efforts to re-invent classical models by taking into account the graph structure, with advances in many problems, such as denoising [5] and semi-supervised learning [6, 7].

Yet, state-of-the-art models for processes (evolving) on graphs often fail to produce useful results when applied to real datasets. One of the main reasons for this shortcoming is that they model only a limited set of (smooth) spatio-temporal behaviors. The well-used graph Tikhonov and total variation priors for instance assume that the signal varies slowly or in a piece-wise constant manner over edges, without specifying any precise relations [8, 9]. Similarly, assuming that the graph Laplacian encodes the conditional correlations of variables, as is done with Gaussian Markov Random Fields [10], works well when the graph is not available, but becomes a rigid model when the graph is given [11]. To capture the

*A. Loukas and N. Perraudin contributed equally to this work.

behavior of complex networked systems, such as transportation and biological networks, it is important to train expressive models, being able to reproduce a wide range of graph and temporal behaviors.

Motivated by this need, this paper considers the statistical modeling of processes evolving on graphs. Our results are inspired by the recent introduction of a joint temporal and graph Fourier transform (JFT), a generalization of GFT appropriate for time-varying graph signals [12], and the recent generalization of stationarity for graphs [13, 14, 15]. Our main contribution is a novel definition of time-vertex wide-sense stationarity, or *joint stationarity* for short. We believe that the proposed definition is natural, as it elegantly relates to existing definitions of stationarity in the time and vertex domains. We show that joint stationarity carries along important properties classically associated with stationarity. Joint wide-sense stationary (JWSS) processes are (a) invariant to a generalization of translation, (b) they can be generated by filtering noise, (c) and a joint Fourier transform diagonalizes their covariance.

We use the assumption of joint stationarity to regularize learning and to reduce computational complexity in both estimation and recovery tasks. We propose scalable estimators that can learn the covariance structure of a JWSS process from $\mathcal{O}(1)$ samples. Moreover, we demonstrate that for JWSS processes one can solve RMSE recovery problems (such as interpolation, denoising, forecasting) in computational complexity that is linear to the number of edges and timesteps.

To test the ability of joint stationarity to capture the properties of complex processes, we apply our methods on three diverse datasets: (a) a meteorological dataset depicting the temperature of 32 weather stations over one month on a mountain top in France, (b) a traffic dataset depicting high resolution daily vehicle flow of 4 weekdays in the highways of Sacramento, and (c) simulated SIRS-type epidemics over Europe. Our experiments suggest that joint stationarity is a useful model, even in datasets which may violate the strict conditions of our definition, and that when few samples it yields an improvement in recovery performance, as compared to time- or vertex-based methods.

1.1 Related work

There exists an extensive literature on multivariate stationary processes, developing the original work of Wiener et al. [16, 17]. The reader may find interesting Bloomberg’s book [18] focusing on the spectral relations. We focus on two main approaches that relate to our work, graphical models and signal processing on graphs.

Graphical models. In the context of graphical models, multivariate stationarity has been used jointly with a graph in the work of [19, 20]. Though relevant, we note that there is a key difference of these models with our approach: we assume that the graph is given, whereas in graphical models the graph structure (or more precisely the precision matrix) is the learned from the data. Knowing the graph allows us to search for more involved relations between the variables. As such, we are not restricted to the case that the conditional dependencies are given by the graph (and therefore that they are sparse), but allow non-adjacent variables to be conditionally dependent, modeling a wider set of behaviors. We also note that our approach is eventually more scalable. We refer to [11] for elements of connections between graphical models and graph signal processing.

Graph signal processing. The idea of studying the stationarity of a random vector with respect to a graph was first introduced by Girault et al. [14, 21] and then by Perraudin et al. [13]. While these contributions have different starting points, they both propose the same definition, i.e., the one we generalize in this contribution. Other recent contributions relating to stationarity on graphs are [15, 22]. Despite the relevance of these works, it is important to stress that this paper is the first to consider processes that are varying both in the vertex and time domains. We also note that the task of prediction using the two first statistical moments for time-evolving signal on graphs was also considered in [23, 24]. Nonetheless, there are a number of differences with these works, with the most important being that we define joint stationarity, and that we are not restricted to the causal case.

It should be noted that an early version of this paper appeared as a technical report [25].

2 Preliminaries

We consider signals supported on the vertices $\mathcal{V} = \{v_1, v_2, \dots, v_N\}$ of a weighted undirected graph $\mathcal{G} = (\mathcal{V}, \mathcal{E}, \mathbf{W}_G)$, with \mathcal{E} the set of edges of cardinality $E = |\mathcal{E}|$ and \mathbf{W}_G the weighted adjacency matrix. A more convenient matrix representation of \mathcal{G} is the (combinatorial¹) Laplacian matrix $\mathbf{L}_G = \text{diag}(\mathbf{W}_G \mathbf{1}_N) - \mathbf{W}_G$, where $\mathbf{1}_N$ is the all-ones vector of size N , and $\text{diag}(\mathbf{W}_G \mathbf{1}_N)$ is the diagonal degree matrix.

¹Though we use the combinatorial Laplacian in our presentation, our results are applicable to any positive semi-definite matrix definition of a graph Laplacian or to the recently introduced shift operator [9].

2.1 Harmonic vertex analysis

In the context of graph signal processing, the importance of the Laplacian matrix stems from it giving rise to a graph-specific notion of frequency. The *Graph Fourier Transform* (GFT) of a graph signal $\mathbf{x} \in \mathbb{R}^N$ is defined as

$$\text{GFT}\{\mathbf{x}\} \triangleq \mathbf{U}_G^* \mathbf{x}, \quad (1)$$

where \mathbf{U}_G is the eigenvector matrix of \mathbf{L}_G and thus $\mathbf{L}_G = \mathbf{U}_G \mathbf{\Lambda}_G \mathbf{U}_G^*$. The GFT allows us to extend filtering to graphs [26, 8, 27]. Denote by (\circ) the element-wise multiplication (Hadamard product). Filtering a signal \mathbf{x} with a graph filter $h(\mathbf{L}_G)$ corresponds to element-wise multiplication in the spectral domain

$$h(\mathbf{L}_G)\mathbf{x} \triangleq \text{GFT}^{-1}\{h(\boldsymbol{\lambda}) \circ \text{GFT}\{\mathbf{x}\}\} = \sum_{n=1}^N h(\lambda_n) \mathbf{u}_n \mathbf{u}_n^* \mathbf{x} \quad (2)$$

where $\boldsymbol{\lambda} = \text{diag}(\mathbf{\Lambda}_G)$ is the vector of graph frequencies, \mathbf{u}_n is the n -th eigenvector of \mathbf{L}_G , and the scalar function $h : \mathbb{R}_+ \mapsto \mathbb{R}$, referred to as the graph frequency response, is applied to each entry of $\boldsymbol{\lambda}$. The notation \mathbf{U}_G^* denotes the transposed complex conjugate of \mathbf{U}_G , \mathbf{U}_G^T the transpose of \mathbf{U}_G , and $(\mathbf{U}_G^*)^\dagger$ the complex conjugate of \mathbf{U}_G .

Graph localization. We will also use the notion of *graph localization* [27, 13], a generalization of the translation operator used in the classical setting appropriate for graphs. Localizing a filter with frequency response h onto vertex v_i reads

$$\mathcal{T}_i^G h \triangleq h(\mathbf{L}_G) \boldsymbol{\delta}_i, \quad (3)$$

where $\boldsymbol{\delta}_i$ is a Kronecker delta centered at vertex v_i . For a sufficiently regular function h , this operation localizes the filter around v_i [27, Theorem 1 and Corollary 2]. Evaluated at the i_2 -th vertex, the above expression becomes

$$[\mathcal{T}_{i_1}^G h](i_2) = \sum_{n=1}^N h(\lambda_n) \mathbf{u}_n^*(i_1) \mathbf{u}_n(i_2), \quad (4)$$

The concept of localization is intimately linked to that of *translation* in the time domain. If $\mathcal{T}_\tau^T h$ is the localization operator taken on a cycle graph of T vertices (representing time), localization is equivalent to translation

$$[\mathcal{T}_\tau^T h](t) = [\mathcal{T}_0^T h](t - \tau), \quad \text{for all } t, \tau = 1, \dots, T. \quad (5)$$

In simple words, for a cyclic graph, the localization operator computes the inverse Fourier transform of the frequency response h , and translates it to vertex v_i . We can verify this using the fact that the complex exponential Fourier basis form the eigenvector set of all cyclic graphs [28], which together with (4) implies that

$$\begin{aligned} [\mathcal{T}_{t_1}^T h](t_2) &= \frac{1}{T} \sum_{\tau=1}^T h(\omega_\tau) e^{-2\pi j \frac{(\tau-1)t_1}{T}} e^{2\pi j \frac{(\tau-1)t_2}{T}} \\ &= \frac{1}{T} \sum_{\tau=1}^T h(\omega_\tau) e^{2\pi j \frac{(\tau-1)(t_2-t_1)}{T}} = [\mathcal{T}_0^T h](t_2 - t_1). \end{aligned} \quad (6)$$

Above $\mathcal{T}_0^T h = \mathbf{U}_T h(\boldsymbol{\lambda}_G)$ is the inverse Fourier transform of $h(\boldsymbol{\lambda}_G)$ and \mathbf{U}_T is the orthonormal Fourier basis. In the case of irregular graphs, localization differs further from translation because the shape of the localized filter adapts to the graph and varies as a function of its topology. Additional insights about the localization operator can be found in [27, 26, 29, 13].

2.2 Harmonic time-vertex analysis

Suppose that a graph signal \mathbf{x}_t is sampled at T successive regular intervals of unit length. The time-varying graph signal $\mathbf{X} = [\mathbf{x}_1, \mathbf{x}_2, \dots, \mathbf{x}_T] \in \mathbb{R}^{N \times T}$ is then the matrix having graph signal \mathbf{x}_t as its t -th column. Equivalently, $\mathbf{X} = [\mathbf{x}^1, \mathbf{x}^2, \dots, \mathbf{x}^N]^\top$ holds N temporal signals $\mathbf{x}^i \in \mathbb{R}^T$, one for each vertex v_i . Throughout this paper, we denote as $\mathbf{x} = \text{vec}(\mathbf{X})$ (without subscript) the vectorized representation of the matrix \mathbf{X} .

Joint Fourier Transform. In matrix and vector forms, the frequency representation of \mathbf{X} , \mathbf{x} is given by the joint (time-vertex) Fourier transform (or JFT for short)

$$\text{JFT}\{\mathbf{X}\} \triangleq \mathbf{U}_G^* \mathbf{X} (\mathbf{U}_T^*)^\top \quad \text{and} \quad \text{JFT}\{\mathbf{x}\} \triangleq (\mathbf{U}_T^* \otimes \mathbf{U}_G^*) \mathbf{x}, \quad (7)$$

with \mathbf{U}_G and \mathbf{U}_T being respectively the graph Laplacian eigenvector matrix and the orthonormal Fourier matrix. It is a known fact that matrix \mathbf{U}_T diagonalizes any Toeplitz matrix, such as the lag operator or the Laplacian matrix of a cyclic graph \mathcal{T} . Denote by $\boldsymbol{\Omega}$ the diagonal matrix of angular frequencies, with $\boldsymbol{\Omega}_{tt} = \omega_t = 2\pi t/T$. When \mathbf{L}_T is the lag operator, we have $\mathbf{L}_T = \mathbf{U}_T e^{-j\boldsymbol{\Omega}} \mathbf{U}_T^*$, where $j = \sqrt{-1}$. Similarly, when the combinatorial Laplacian is used, $\mathbf{L}_T = \mathbf{U}_T \text{real}(\mathbf{I} - e^{-j\boldsymbol{\Omega}}) \mathbf{U}_T^*$. It is perhaps more intuitive to think of the JFT of \mathbf{x} on a graph \mathcal{G} as the GFT of the same signal on a new graph, called the *joint graph* \mathcal{J} , that is the graph cartesian product of \mathcal{G} and a cyclic graph \mathcal{T} . Denote by (\otimes) the Kronecker product and let \mathbf{I}_C be the identity matrix of size $C \times C$. The Laplacian of the joint graph, which is equal to $\mathbf{L}_J = \mathbf{L}_T \otimes \mathbf{I}_N + \mathbf{I}_T \otimes \mathbf{L}_G$, has eigenvectors $\mathbf{U}_J = \mathbf{U}_T \otimes \mathbf{U}_G$ and eigenvalues $\boldsymbol{\Lambda}_J = \boldsymbol{\Lambda}_T \otimes \mathbf{I}_N + \mathbf{I}_T \otimes \boldsymbol{\Lambda}_G$. As such, we can write $\text{JFT}\{\mathbf{x}\} = \mathbf{U}_J^* \mathbf{x}$. For an in-depth discussion of JFT and its properties, we refer the reader to [12].

Joint time-vertex filtering. Leveraging the definition of JFT, filtering can also be extended to the joint (time-vertex) domain. Filtering a signal \mathbf{x} with a *joint filter* $h(\mathbf{L}_J)$ corresponds to element-wise multiplication in the joint spectral domain $\vartheta = [\lambda, \omega]$ (λ denotes the graph eigenvalues and ω the angular frequencies) by a function $h : \mathbb{R}_+ \times \mathbb{R} \mapsto \mathbb{R}$. When a joint filter $h(\mathbf{L}_J)$ is applied to \mathbf{x} , the output is

$$h(\mathbf{L}_J)\mathbf{x} \triangleq \text{vec}(\text{JFT}^{-1}\{h(\boldsymbol{\Theta}) \circ \text{JFT}\{\mathbf{X}\}\}), \quad (8)$$

where $\boldsymbol{\Theta}_{n,\tau} = \vartheta_{n,\tau} = [\lambda_n, \omega_\tau]$ is an $N \times T \times 2$ tensor, and $h(\boldsymbol{\Theta})$ is a diagonal $NT \times NT$ matrix with $[h(\boldsymbol{\Theta})]_{n,\tau} = h(\vartheta_{n,\tau})$. Furthermore, we say that a joint filter is *separable*, if its joint frequency response $h(\vartheta)$ can be written as the product of a frequency response defined solely in the vertex domain and one in the time domain, which implies that

$$h(\mathbf{L}_J)\mathbf{x} = (h_1(\mathbf{L}_T) \otimes h_2(\mathbf{L}_G)) \mathbf{x}, \quad (9)$$

with $h(\vartheta) = h_1(\omega) \cdot h_2(\lambda)$. We note that $h(\mathbf{L}_J)$ is not strictly a matrix function of \mathbf{L}_J as $h(\cdot, \cdot)$ does not act on the diagonal entries $[\boldsymbol{\Lambda}_J]_{kk}$ of the eigenvalue matrix of \mathbf{L}_J (which are 1 dimensional), but on $\vartheta_{n,\tau} = [\lambda_n, \omega_\tau]$.

3 Joint Time-Vertex Stationarity

Let $\mathbf{X} \in \mathbb{R}^{N \times T}$ be a discrete multivariate stochastic process with finite number of time-steps T that is indexed by the vertex v_i of graph \mathcal{G} and time t . We refer to such processes as joint time-vertex processes, or *joint processes* for short.

Our objective is to provide a definition of stationarity that captures statistical invariance of the first two moments of a joint process $\mathbf{x} = \text{vec}(\mathbf{X}) \sim \mathcal{D}(\bar{\mathbf{x}}, \boldsymbol{\Sigma}_{\mathbf{x}})$, i.e., the mean $\bar{\mathbf{x}} = \mathbf{E}[\mathbf{x}]$ and the covariance $\boldsymbol{\Sigma}_{\mathbf{x}}$ under distribution \mathcal{D} . Crucially, the definition should do so in a manner that is faithful to the graph structure. That is, if we express the covariance as

$$\boldsymbol{\Sigma}_{\mathbf{x}} = \begin{pmatrix} \boldsymbol{\Gamma}(1,1) & \boldsymbol{\Gamma}(1,2) & \cdots & \boldsymbol{\Gamma}(1,T) \\ \boldsymbol{\Gamma}(2,1) & \boldsymbol{\Gamma}(2,2) & & \\ \vdots & & \ddots & \vdots \\ \boldsymbol{\Gamma}(T,1) & & \cdots & \boldsymbol{\Gamma}(T,T) \end{pmatrix}$$

the statistical relation of variables at a given time-step $\boldsymbol{\Gamma}(t_1, t_1)$ and those across different timesteps $\boldsymbol{\Gamma}(t_1, t_2)$ should be a function of the graph Laplacian.

It is helpful to briefly consider the classical case of a univariate time wide-sense stationary (TWSS) process ($N = 1$). Every TWSS process has three equivalent properties: (a) it can be generated by filtering white noise, (b) the process is uncorrelated in the spectral domain, and (c) its first two moments are invariant to translation in the time dimension.

We argue that these properties can be extended to joint processes as follows:

Definition 1 (Joint stationarity). *A joint process $\mathbf{x} = \text{vec}(\mathbf{X})$ is called Jointly Wide-Sense Stationary (JWSS), if any of the following hold:*

- (a) The process is generated by filtering $\varepsilon \sim \mathcal{D}(\mathbf{c}, \mathbf{I}_{NT})$ with a joint filter such that $\mathbf{x} = h^{\frac{1}{2}}(\mathbf{L}_J)\varepsilon$, where $\mathbf{L}_J\mathbf{c} = \mathbf{0}$.
- (b) The variables in the joint spectral domain are independent and have zero mean, except for the DC component (the null space of \mathbf{L}_J). Equivalently, $\Sigma_{\mathbf{x}}$ is jointly diagonalizable with \mathbf{L}_J .
- (c) The expected value is in the null space of the Laplacian $\mathbf{L}_J\bar{\mathbf{x}} = \mathbf{0}_{NT}$, and for all $\tau = t_2 - t_1$ there exists a series of graph filters $\gamma_{\tau}(\lambda)$, such that $\mathbf{\Gamma}(t_1, t_2) = \mathbf{\Gamma}(1, 1 + t_2 - t_1) = \gamma_{\tau}(\mathbf{L}_G)$.

As the following Theorem claims (all proofs are deferred to the appendix) statements (a-c) are equivalent.

Theorem 1. *If a process \mathbf{X} satisfies statement (a), (b) or (c) in Definition 1, then it satisfies all of them.*

Let us examine Definition 1 in detail.

First moment conditions. The definition claims that “the expected value of any JWSS process is in the null space of the Laplacian $\mathbf{L}_J\bar{\mathbf{x}} = \mathbf{0}_{NT}$ ”. In the case where \mathbf{L}_G is the combinatorial Laplacian, this statement simplifies to the familiar requirement that the mean has to be constant over the time and the vertex sets ($\bar{\mathbf{X}}_{i,t} = c$). That is because for a connected graph, the null space of the combinatorial Laplacian consists of a unique constant vector. By postulating our assumption in terms of the null space of \mathbf{L}_J , we can generalize first moment invariance to alternative matrix representations, such as the normalized Laplacian.

Second moment conditions. Statements (a-b) are directly analogous to the classical case, with the Fourier transform being generalized by JFT and filtering by joint filtering. The third statement is more involved. It enforces two properties on the covariance matrix of a JWSS process: First, similar to time stationary processes, $\Sigma_{\mathbf{x}}$ should possess a block Toeplitz structure, by imposing $\mathbf{\Gamma}(t_1, t_2) = \mathbf{\Gamma}(t_1 - t_2 + 1, 1)$. This implies that the correlations only depend on the time difference $t_1 - t_2 = \tau$ and not on any time localization. Second, similar to vertex stationarity each block of $\Sigma_{\mathbf{x}}$ should be jointly diagonalizable with the graph Laplacian \mathbf{L}_G (see the work of Perraudin and Vandergheynst [13]). A closer look into statement (a) and (c) reveals a further connection. Assuming that a process is JWSS is equivalent to stating that its covariance matrix is the linear filter $\Sigma_{\mathbf{x}} = h(\mathbf{L}_J)$, where

$$\gamma_{\tau}(\lambda) = \frac{1}{T} \sum_{t=1}^T h(\lambda, \omega_t) e^{i\omega_t\tau}. \quad (10)$$

Furthermore, $\Sigma_{\text{JFT}\{\mathbf{x}\}} = \text{diag}(h(\Theta))$, which can be seen a generalization the Wiener-Khintchine relation, where $h(\vartheta)$ plays the role of the PSD. In fact, it is the autocorrelation function of signal \mathbf{x} viewed from the joint Fourier domain. To this end, we refer to it as time-vertex power spectral density or *Joint Power Spectral Density* (JPSD) for short.

3.1 Relations to classical definitions

We next provide a rigorous examination of the relations between joint stationarity, the classical definition of time stationarity and that of vertex stationarity. Although our exposition is self-contained, the reader will benefit from familiarizing with previous work on stationarity for graphs [13]

JWSS \subset TWSS. Let us recall the notion of time stationarity for multivariate processes.

Definition 2 (Multivariate time stationarity). *A joint process \mathbf{X} is Time Wide-Sense Stationary (MTWSS), if and only if the following two properties hold*

- (a) The expected value is constant as $\bar{\mathbf{x}}_t = \mathbf{c}$ for all t .
- (b) For all t_1, t_2 the second moment satisfies $\mathbf{\Gamma}(t_1, t_2) = \mathbf{\Gamma}(t_1 - t_2 + 1, 1) = \mathbf{\Gamma}(\tau)$, where $\tau = t_1 - t_2$.

This definition implies that $\Sigma_{\mathbf{x}}$ is block Toeplitz. From (c) in Definition 1, we observe that joint stationarity is a particular case of multivariate time stationarity.

Similarly to the univariate case, we can define a Time Power Spectral Density (TPSD) to encode the statistics of the signal in the spectral domain.

$$\hat{\mathbf{\Gamma}}(\omega) = \frac{1}{\sqrt{T}} \sum_{\tau=1}^T \mathbf{\Gamma}(\tau) e^{-i\omega(\tau-1)}$$

For a JWSS process, we observe that $\hat{\Gamma}(\omega) = h_\omega(\mathbf{L}_G)$, where $h_\omega = h(\lambda, \omega)$.

JWSS \subset VWSS. The concept of stationarity has been generalized to graph signals [13]. This contribution states that a random signal is stationary on a graph if its expected value is constant on the vertex set, and the covariance matrix is jointly diagonalizable with the Laplacian, i.e., $\Sigma_{\mathbf{x}_t} = h(\mathbf{L}_G)$. This notion of stationarity does not apply to time evolving processes as it does not characterize the correlation between different time-steps. As a result, we present here a generalization of this framework to the temporal series on graph.

Definition 3 (Multivariate vertex stationarity). *A joint process $\mathbf{X} = [\mathbf{x}_1 \mathbf{x}_2 \dots \mathbf{x}_T]$ is called Multivariate Vertex Wide-Sense (or second order) Stationary (MVWSS), if and only if the following two properties hold independently:*

- (a) *The expected value is in the null space of the Laplacian $\mathbf{L}_G \bar{\mathbf{x}}_t = \mathbf{0}_N, \forall t$.*
- (b) *For all t_1 and t_2 , we have $\Gamma(t_1, t_2) = \gamma_{t_1, t_2}(\mathbf{L}_G)$.*

Similar to the definition of joint stationarity, Definition 3 asserts that every covariance matrix $\Gamma(t_1, t_2)$ is jointly diagonalizable with the graph Laplacian. Unlike JWSS processes however, here $\Gamma(t_1, t_2) \neq \Gamma(t_1 - t_2 + 1, 1)$.

JWSS = TWSS \cap VWSS. As shown next, the two definitions taken together are equivalent to that of joint stationarity.

Theorem 2. *A joint process \mathbf{X} is JWSS if and only if it is both MTWSS and MVWSS.*

In other words, the set of processes that are JWSS are exactly those that are statistically invariant in the temporal and vertex domains.

3.2 Further properties

We briefly present two additional properties of JWSS processes that will be useful in the rest of the paper.

Property 1 (White noise). *White centered i.i.d. noise $\mathbf{w} \in \mathbb{R}^{NT} \sim \mathcal{D}(\mathbf{0}_{NT}, \mathbf{I}_{NT})$ is JWSS with constant JPSD for any graph.*

The proof follows easily by noting that white noise satisfies point (b) of Definition 1: The covariance of \mathbf{w} is diagonalized by the joint Fourier basis of any graph $\Sigma_{\mathbf{w}} = \mathbf{I} = \mathbf{U}_J \mathbf{I} \mathbf{U}_J^*$. This last equation tells us that the JPSD is constant, which implies that similar to the classical case, white noise contains all joint (time-vertex) frequencies.

A second interesting property of JWSS processes is that stationarity is preserved through a filtering operation.

Property 2. *When a joint filter $f(\mathbf{L}_J)$ is applied to a JWSS process \mathbf{X} , the result \mathbf{Y} remains JWSS with mean $f(0, 0)\mathbf{E}[\mathbf{X}]$ and JPSD $f^2(\vartheta_{n, \tau}) h_{\mathbf{x}}(\vartheta_{n, \tau})$.*

4 Joint Power Spectral Density estimation

The joint stationarity assumption can be very effective in overcoming the challenges associated with dimensionality. The main reason is that, for JWSS processes, the estimation variance is decoupled from the problem size. Concretely, suppose that we want to estimate the covariance matrix $\Sigma_{\mathbf{x}}$ of a joint process $\mathbf{x} = \text{vec}(\mathbf{X})$ from K samples $\mathbf{x}_{(1)}, \mathbf{x}_{(2)}, \dots, \mathbf{x}_{(K)}$. As we show in the following, if the process is JWSS such that $\Sigma_{\mathbf{x}} = h(\mathbf{L}_J)$, estimation is possible from $K = \mathcal{O}(1)$ samples! This is a sharp decrease from the classical and TWSS settings, for which $K \approx NT$ and $K \approx N$ samples are necessary², respectively.

This section presents two JPSD estimators requiring constant number of samples. The first provides unbiased estimates at complexity that is $\mathcal{O}(N^3 T \log(T))$. The second estimator, decreases further the estimation variance at a cost of a bounded bias, and can be approximated at complexity linear to ET .

²The number of samples needed for obtaining a good sample covariance matrix of an n -dimensional process is $\mathcal{O}(n \log n)$ [1, 30].

4.1 Sample JPSD estimator

We define the ‘‘sample JPSD estimator’’ for every graph frequency λ and temporal frequency ω as the estimate

$$\hat{h}(\vartheta) \triangleq \sum_{k=1}^K \frac{(\mathbf{u}^* \mathbf{x}_{(k)})^2}{K}. \quad (11)$$

with \mathbf{u} the joint basis eigenvector corresponding to eigenvalues $\vartheta = (\lambda, \omega)$. Let $\mathbf{x}_{(k)} = h(\mathbf{L}_J)^{1/2} \boldsymbol{\varepsilon}_{(k)}$, where random vector $\boldsymbol{\varepsilon}_{(k)}$, is zero mean and identity covariance. The sample estimate can be rewritten as

$$\begin{aligned} \hat{h}(\vartheta) &= \sum_{k=1}^K \frac{\mathbf{x}_{(k)}^* \mathbf{u} \mathbf{u}^* \mathbf{x}_{(k)}}{K} \\ &= \sum_{k=1}^K \frac{\boldsymbol{\varepsilon}_{(k)}^* h(\mathbf{L}_J)^{1/2} \mathbf{u} \mathbf{u}^* h(\mathbf{L}_J)^{1/2} \boldsymbol{\varepsilon}_{(k)}}{K} = h(\vartheta) \sum_{k=1}^K \frac{\hat{\varepsilon}_{(k)}^2}{K}, \end{aligned}$$

with every realization of $\hat{\varepsilon} = \mathbf{u}^* \boldsymbol{\varepsilon}$ being an independent zero mean random variable with unit variance. It is an immediate consequence that the sample JPSD estimator is unbiased with a variance that depends on the fourth order moment of $\hat{\varepsilon}$.

Theorem 3. *For every distribution with bounded second and fourth order moments, the sample JPSD estimator $\hat{h}(\vartheta)$*

(a) *is unbiased, $\mathbf{E}[\hat{h}(\vartheta)] = h(\vartheta)$, and*

(b) *has variance $\mathbf{Var}[\hat{h}(\vartheta)] = h^2(\vartheta) \frac{\mathbf{E}[\hat{\varepsilon}^4] - 1}{K}$.*

For the special case of a Gaussian distribution, $\hat{\varepsilon}^2$ is a chi-squared distribution with 1 degree of freedom, meaning that our estimate follows a Gamma distribution.

Corollary 1. *For every Gaussian JWSS process, the sample JPSD estimate follows a Gamma distribution with shape $K/2$ and scale $2h(\vartheta)/K$. The estimation error variance is equal to $\mathbf{Var}[\hat{h}(\vartheta) - h(\vartheta)] = 2h^2(\vartheta)/K$.*

Observe that the variance depends linearly on the fourth order moment of $\hat{\varepsilon}$ and is inversely proportional to the number of samples, but it is independent on N or T . In the following, we show how to achieve an even smaller variance by exploiting the properties of $h(\vartheta)$. In addition, we reduce the estimation accuracy by avoiding to perform an eigenvalue decomposition.

4.2 Convolutional JPSD estimator

When the number of available signals K is small (even 1), we need an additional assumption on the correlations to obtain reasonable estimates.

Before delving into JWSS processes, it is helpful to consider the purely temporal case. For a TWSS process it is customary to assume that the autocorrelation function has support L that is a few times smaller than T . Then, cutting the signal into $\frac{T}{L}$ smaller parts and computing the average estimate, reduces the variance (by a factor of $\frac{T}{L}$), without sacrificing frequency resolution. This basic idea stems from two established methods used to estimate the PSD of a temporal signal, namely Bartlett’s and Welch’s methods [31, 32]. The act of averaging across different windows is in fact equivalent to a convolution in the spectral domain. Convoluting the TPSD with a window, results in attenuation of the correlation for large delays, enforcing localization in the time domain.

Motivated by the observation that convolution with a window in the graph frequency domain also encourages localization in the vertex domain [27, Theorem 1 and Corollary 2], we propose to reduce the estimation variance by convoluting the sample JPSD. Concretely, Let $g(\vartheta)$ be a 2D window defined in the joined frequency domain. We define our convolutional JPSD estimator as

$$\ddot{h}(\vartheta) \triangleq \frac{1}{c_g(\vartheta)} \sum_{\substack{n=1 \\ \tau=1}}^{N,T} g(\vartheta - \vartheta_{n,\tau})^2 \hat{h}(\vartheta_{n,\tau}), \quad (12)$$

where, $c_g(\vartheta) \triangleq \sum_{n=1, \tau=1}^{N, T} g(\vartheta - \vartheta_{n, \tau})^2$ is a normalization factor that depends on the $\vartheta = (\lambda, \omega)$ frequency pair (since the graph eigenvalues are generally irregularly spaced). Moreover, $\dot{h}(\vartheta_{n, \tau})$ is the sample estimate defined in (11).

The convolutional JPSD estimator is a generalization of known PSD estimators for TWSS and GWSS processes. Denote by δ the dirac function. We have that: (a) For $g(\vartheta) = \delta(\lambda) \cdot g_T(\omega)$, we recover the classical TPSD estimator, applied independently for each λ . (b) For $g(\vartheta) = g_G(\lambda) \cdot \delta(\omega)$, we recover the GPSD estimator from [13] applied independently for each ω .

To provide a meaningful bias analysis, we introduce a Lipschitz continuity assumption on the JPSD, matching the intuition that localized phenomena tend to have a smooth representation in the frequency domain.

Theorem 4. *For any distribution with bounded second and fourth order moments, the convolutional estimator $\ddot{h}(\vartheta)$*

(a) *has bias*

$$\left| \mathbf{E} \left[\ddot{h}(\vartheta) - h(\vartheta) \right] \right| \leq \frac{\epsilon}{c_g(\vartheta)} \sum_{n=1, \tau=1}^{T, N} g(\vartheta - \vartheta_{n, \tau})^2 \|\vartheta - \vartheta_{n, \tau}\|_2,$$

where ϵ is the Lipschitz constant of $h(\vartheta)$, and

(b) *has variance*

$$\mathbf{Var} \left[\ddot{h}(\vartheta) \right] = \sum_{n, \tau}^{N, T} \frac{g(\vartheta - \vartheta_{n, \tau})^4}{c_g(\vartheta)^2} h(\vartheta_{n, \tau})^2 \frac{\mathbf{E} \left[\hat{\epsilon}_{n, \tau}^4 \right] - 1}{K}.$$

The derivations of the bias and variance are given in Lemmas 1 and 2, respectively.

For the standard case of a Gaussian distribution and of a disc window with bandwidth B , i.e., $g_B(\vartheta) = 1$ if $\|\vartheta\|_2 \leq \frac{B}{2}$ and 0 otherwise, the bias and variance expressions simplify considerably.

Corollary 2. *For every ϵ -Lipschitz Gaussian JWSS process and disc window $g_B(\theta)$, the convolutional estimate has*

$$\left| \mathbf{E} \left[\ddot{h}(\vartheta) - h(\vartheta) \right] \right| \leq \frac{\epsilon B}{2} \quad \text{and} \quad \mathbf{Var} \left[\ddot{h}(\vartheta) \right] = \frac{2 h_{\mathcal{S}}^2}{K |\mathcal{S}|}, \quad (13)$$

with set $\mathcal{S} = \{\vartheta_{n, \tau} \mid \|\vartheta_{n, \tau} - \vartheta\|_2 \leq B/2\}$ and $h_{\mathcal{S}}^2 = \sum_{\vartheta_{n, \tau} \in \mathcal{S}} \frac{h(\vartheta_{n, \tau})^2}{|\mathcal{S}|}$.

Therefore, by selecting our window (bandwidth) we can trade-off bias for variance. The trade-off is particularly beneficial as long as (a) the JPSD is smooth, and (b) the graph eigenvalues are clustered, such that $|\mathcal{S}| \gg B$.

4.3 Fast implementation

Having defined the convolutional JPSD estimator, we turn to its computation. A straightforward implementation requires (a) $\mathcal{O}(N^3)$ operations for computing the eigenbasis of our graph, (b) $\mathcal{O}(N^2 T)$ for performing T independent GFT, (c) $\mathcal{O}(NT \log(T))$ for N independent FFT, and (d) $\mathcal{O}(N^2 T^2)$ for the convolution.

This section describes how to approximate a convolutional estimate using a number of operations that is linear to ET . To do so, it helps to assume that the convolution window is separable, i.e., $g(\vartheta) = g_G(\lambda) \cdot g_T(\omega)$. The benefit of separable windows is that the joint convolution can be performed independently (and at any order) in the time and vertex domain

$$\ddot{h}(\vartheta) = \sum_{\tau=1}^T \frac{g_T(\omega - \omega_{\tau})^2}{c_{g_T}(\omega)} \sum_{n=1}^N \frac{g_G(\lambda - \lambda_n)^2}{c_{g_G}(\lambda)} \dot{h}(\vartheta_{n, \tau}), \quad (14)$$

where $c_g(\vartheta) = c_{g_T}(\omega) \cdot c_{g_G}(\lambda)$. Exploiting this property, we treat the implementation of the two convolutions separately and the presented algorithms can be combined in any order.

Fast time convolution. This is the textbook case of TPSD estimation, that is solved by the Welch’s method [32]. The method entails splitting each timeseries into equally sized overlapping segments, and averaging over segments the squared amplitude of the Fourier coefficients. The procedure is equivalent to an averaging (over time) of the squared coefficients of a Short Time Fourier Transform (STFT), with half overlapping windows w_T defined such that $\text{DFT}\{w_T(t)\} = g_T(\omega)$ [33, 34]. Let L be the support of the autocorrelation, or equivalently the number of frequency bands. We suggest using the iterated sine window

$$w_T(t) \triangleq \begin{cases} \sin\left(0.5\pi \cos(\pi t/L)^2\right) & \text{if } t \in [-L/2, L/2] \\ 0 & \text{otherwise,} \end{cases}$$

as it turns the STFT into a tight operator. In order to get an estimate of \dot{h} at unknown frequencies, we interpolate between the L known points using splines [35]. Whenever L is larger or equal to the autocorrelation support, the above method is exact—no approximation error is introduced.

Fast graph convolution. Inspired by the technique of [13], we perform the graph convolution using an approximated graph filtering operation [36] that scales linearly to the number of graph edges E . In particular,

$$\sum_{n=1}^N \frac{g_G(\lambda - \lambda_n)^2}{c_{g_G}(\lambda)} \dot{h}(\vartheta_{n,\tau}) = \frac{\|g_G(\mathbf{L}_G - \lambda \mathbf{I}_N) \mathbf{x}_\tau\|_2^2}{c_{g_G}(\lambda)}. \quad (15)$$

We suggest using the Gaussian window

$$g_G(\lambda_n - \lambda) \triangleq e^{-(\lambda_n - \lambda)^2/\sigma^2}, \quad (16)$$

with $\sigma^2 = 2(F + 1)\lambda_{\max}/F^2$. As we did before, we only compute the above for $F = \mathcal{O}(1)$ different values of λ and approximate the rest using splines. As the eigenvalues are not known, we need a stable way to estimate $c_{g_G}(\lambda)$. We obtain an unbiased estimate by filtering $Q = \mathcal{O}(1)$ random Gaussian signals on the graph $\boldsymbol{\varepsilon} \in \mathbb{R}^N \sim \mathcal{N}(0, \mathbf{I}_N)$, such that

$$c_{g_G}(\lambda) = \mathbf{E} \left[\sum_{q=1}^Q \|g_G(\mathbf{L}_G - \lambda \mathbf{I}_N) \boldsymbol{\varepsilon}_{(q)}\|_2^2 \right], \quad (17)$$

with variance equal to $2 \sum_{n=1}^N g^4(\lambda_n - \lambda)/Q$. We omit the analysis, as it is similar to those in Theorems 3 and 4. According to our numerical evaluation, the approximation error introduced by the latter estimator and spectral filtering is almost negligible for smooth JPSD.

Complexity. Combining the preceding methods, the cost is reduced to (a) $\mathcal{O}((T + Q)FE)$ for the fast graph convolution, and (b) $\mathcal{O}(NT \log(L))$ for the fast time convolution (for N STFT), yielding a total complexity of $\mathcal{O}(TFE + NT \log(L))$. We remark that, though asymptotically superior, the fast implementation can be significantly slower when the number of variables is small. Our experiments demonstrate that it should be preferred for N, T larger than a few thousands (see Figure 2).

5 Recovery of JWSS Processes

This section considers the MMSE problem of recovering a hidden process $\mathbf{x} = \text{vec}(\mathbf{X})$ from linear measurements $\mathbf{y} = \mathbf{A}\mathbf{x} + \mathbf{w}$, defined as

$$\begin{aligned} \hat{\mathbf{x}} &= \arg \min_{\mathbf{z} \in \mathbb{R}^N} \mathbf{E} [\|\mathbf{z} - \mathbf{x}\|_2^2] \\ \text{subject to} & \quad \mathbf{z} - \bar{\mathbf{x}} \sim \mathcal{D}_1(\mathbf{0}, h_{\mathbf{x}}(\mathbf{L}_J)) \\ & \quad \mathbf{w} \sim \mathcal{D}_2(\mathbf{0}, h_{\mathbf{w}}(\mathbf{L}_J)). \end{aligned} \quad (\text{P0})$$

Above, \mathcal{D}_1 and \mathcal{D}_2 are distributions with finite second order moments, and \mathbf{A} is a general linear operator. We remark that (a) for \mathbf{A} diagonal and binary, (P0) is an *interpolation* problem, (b) for \mathbf{A} diagonal with $\mathbf{A}_{ii} = 1$ if $i \leq Nt$ and zero otherwise it corresponds to *forecasting*, and (c) for $\mathbf{A} = \mathbf{I}$ to *denoising*.

Though the literature abounds with solutions to MMSE problems, the complexity of known algorithms becomes prohibitive for large problems when $\boldsymbol{\Sigma}_{\mathbf{y}}$ is not sparse and ill-conditioned. To exemplify this,

consider the simple case where $\bar{\mathbf{x}} = \mathbf{0}$ and \mathbf{w} is white noise. Computing the *minimum mean-squared linear estimate*

$$\hat{\mathbf{x}}|\mathbf{y} = \Sigma_{\mathbf{x}|\mathbf{y}}\Sigma_{\mathbf{y}}^{-1}\mathbf{y}. \quad (18)$$

involves the solution of a linear system in matrix $\Sigma_{\mathbf{y}} = \mathbf{A}\Sigma_{\mathbf{x}}\mathbf{A}^*$, and has complexity of $\mathcal{O}(N^2T^2)$. Moreover, the number of iterations of conjugate gradient methods increases as $\mathcal{O}(\sqrt{\kappa})$, where the condition number κ of $\Sigma_{\mathbf{y}}$ can be very large in practice.

5.1 Scalable MMSE recovery.

As we show next, by exploiting the joint stationarity assumption, (P0) can be solved in $\mathcal{O}(ET + NT \log(T))$ operations. The crux of our argument is that, even if matrices $h_{\mathbf{x}}(\mathbf{L}_J)$ and $h_{\mathbf{w}}(\mathbf{L}_J)$ are not sparse, their multiplication with a vector is well approximated by spectral filtering on the underlying graph [36]. We can therefore use the sparsity of the graph representation in order to facilitate processing. Moreover, we overcome the bad conditioning issue by employing iterative methods for non-smooth functions.

Instead of solving the recovery problem directly, our approach will be to consider two alternative convex optimization problems, which -under specific conditions- will be shown to correspond to solutions of (P0). The iterative minimizers of the two problems are given at the end of the section. Depending on whether $\text{tr}(\Sigma_{\mathbf{w}}) \neq 0$ (noisy) or $\text{tr}(\Sigma_{\mathbf{w}}) = 0$ (noise-less), we consider respectively problems

$$\begin{aligned} \hat{\mathbf{x}} = \arg \min_{\mathbf{z} \in \mathbb{R}^N} \quad & \|\mathbf{A}\mathbf{z} - \mathbf{y}\|_2^2 + \|f(\mathbf{L}_J)(\mathbf{z} - \bar{\mathbf{x}})\|_2^2 \\ \text{where} \quad & f(\mathbf{L}_J) \triangleq h_{\mathbf{w}}(\mathbf{L}_J)^{1/2} h_{\mathbf{x}}(\mathbf{L}_J)^{-1/2}. \end{aligned} \quad (P1)$$

or in the noise-less case,

$$\begin{aligned} \hat{\mathbf{x}} = \arg \min_{\mathbf{z} \in \mathbb{R}^N} \quad & \|h_{\mathbf{x}}^{-1/2}(\mathbf{L}_J) (\mathbf{z} - \bar{\mathbf{x}})\|_2^2 \\ \text{subject to} \quad & \mathbf{A}\mathbf{z} = \mathbf{y}. \end{aligned} \quad (P2)$$

To gain intuition, we notice that the *joint Fourier penalization weights* $f(\vartheta)$ can be re-written as $f(\vartheta) = (\text{SNR}(\vartheta))^{-1/2}$, and therefore penalize frequencies associated with low SNR and vice-versa. Note that if $h_{\mathbf{x}}(\vartheta) = 0$ for a given ϑ , the associated frequency will be penalized with an infinite weight. As a result, the minimization process will force this frequency component to 0. As another important consequence of this, the operator $f(\mathbf{L}_J)$ is not differentiable and thus Problems (P1) and (P2) cannot be solved using gradient techniques. We will show later how to circumvent this issue.

Equivalence results. We provide three equivalence results between the solution of Problems (P1) and (P2) and standard estimators. Our theoretical derivations consider the case where $\Sigma_{\mathbf{x}} = h_{\mathbf{x}}(\mathbf{L}_J)$ and $\Sigma_{\mathbf{y}} = \mathbf{A}h_{\mathbf{x}}(\mathbf{L}_J)\mathbf{A}^* + h_{\mathbf{w}}(\mathbf{L}_J)$ are invertible. This assumption is not necessary for correctness, but greatly simplifies our task. To begin with, when the noise is white, the two optimization problems are linear minimum mean squared estimators.

Theorem 5. *If \mathbf{x} is JWSS with PSD $h_{\mathbf{x}}(\mathbf{L}_J)$ and \mathbf{w} is i.i.d white noise with $h_{\mathbf{w}}(\mathbf{L}_J) = \sigma^2\mathbf{I}$, then the solutions of Problems (P1) and (P2) are the linear minimum mean squared estimators for (P0).*

It is known in estimation theory that for Gaussian processes the linear minimum mean squared estimator is equivalent to the maximum a posteriori estimator.

Corollary 3. *If $\mathbf{x} \sim \mathcal{N}(\mathbf{0}, h_{\mathbf{x}}(\mathbf{L}_J))$ and $\mathbf{w} \sim \mathcal{N}(\mathbf{0}, \sigma^2\mathbf{I})$ are JWSS Gaussian processes, then the solutions of Problems (P1) and (P2) are MAP estimators for $\mathbf{x}|\mathbf{y}$.*

We can obtain an even stronger result under an alternative assumption.

Theorem 6. *If \mathbf{x} and \mathbf{w} are JWSS, and if the operator \mathbf{A} is jointly diagonalizable with \mathbf{L}_J , such that $\mathbf{A} = a(\mathbf{L}_J)$, then the solutions of Problems (P1) and (P2) are equal to the solution of (P0).*

The conditions of Theorem 6 are met for instance in denoising, where $\mathbf{A} = \mathbf{I}$. Furthermore, the theorem holds for any distribution \mathcal{D}_1 and \mathcal{D}_2 . The proofs are generalizations of classical results in signal processing and machine learning (see also [13]). For clarity, we defer them to the Appendix.

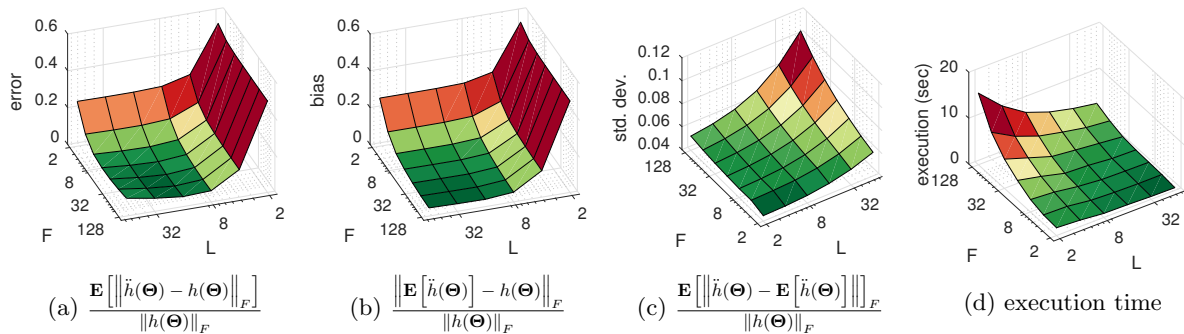


Figure 1: Influence of the parameters (window size L and number of graph filters F) on the estimation error (a), bias (b), normalized std. dev. (c), and execution time (d). For improved visibility, the direction of the axes in (c-d) have been reversed.

Algorithms. We focus first on the noisy case. In general Problem (P1) cannot be solved using the conjugate gradient method because $f(\mathbf{L}_J)$ is often badly conditioned (when $h_{\mathbf{x}}(\lambda, \omega)$ is close to 0). Fortunately, thanks to proximal splitting methods, we can derive a stable algorithm for solving Problem (P1) that requires only the application of \mathbf{A} and spectral graph filtering.

We employ an accelerated forward-backward splitting scheme [37], with term $\|\mathbf{A}\mathbf{x} - \mathbf{y}\|_2^2$ as the differentiable function. The proximal operator of $\|f(\mathbf{L}_J)(\mathbf{x} - \bar{\mathbf{x}})\|_2^2$ is

$$\begin{aligned} & \text{prox}_{\frac{1}{2}} \|f(\mathbf{L}_J)(\mathbf{z} - \bar{\mathbf{x}})\|_2^2(\mathbf{u}) \\ &= \bar{\mathbf{x}} + \arg \min_{\mathbf{z}} \|f(\mathbf{L}_J) \text{JFT}\{\mathbf{z}\}\|_2^2 + \|\mathbf{z} - \mathbf{u} + \bar{\mathbf{x}}\|_2^2 \\ &= \bar{\mathbf{x}} + g(\mathbf{L}_J)(\mathbf{u} - \bar{\mathbf{x}}) \end{aligned}$$

where

$$g(\vartheta) \triangleq \frac{1}{1 + f(\vartheta)} = \frac{h_{\mathbf{x}}(\vartheta)}{h_{\mathbf{x}}(\vartheta) + h_{\mathbf{w}}(\vartheta)} \quad (19)$$

and $\frac{0}{0} = 0$. Interestingly, this proximal operator is equivalent to a joint wiener filter. The full fledged optimization scheme is given in Algorithm 1. We set the step size to $\beta = \lambda_{\max}(\mathbf{A})^{-2}$. Also, ϵ is the stopping tolerance, J is the maximum number of iterations, and δ is a very small number that helps avoid division by 0. Problem P2 is solved similarly with a Douglas-Rachford scheme [38].

Algorithm 1 Accelerated optimization scheme for (P1)

Require: $\epsilon > 0$, $\beta \leq \lambda_{\max}(\mathbf{A})^{-2}$, $J > 0$

Set $\mathbf{z}_1 = \mathbf{x}$, $\mathbf{u}_0 = \mathbf{x}$, $t_1 = 1$

▷ Initialization

Design filter $g(\mathbf{L}_J)$ such that $g(\lambda, \omega) = \frac{h_{\mathbf{x}}(\lambda, \omega)}{h_{\mathbf{x}}(\lambda, \omega) + h_{\mathbf{w}}(\lambda, \omega)}$.

for $j = 1, \dots, J$ **do**

$\mathbf{v} = \mathbf{z}_j - \beta \mathbf{A}^*(\mathbf{A}\mathbf{z}_j - \mathbf{y})$

▷ Gradient step $\mathcal{O}(\|\mathbf{A}\|_0)$

$\mathbf{u}_{j+1} = g(\mathbf{L}_J) \mathbf{v}$

▷ Proximal step $\mathcal{O}(ET)$

$t_{j+1} = 0.5 \cdot (1 + \sqrt{1 + 4t_j^2})$

▷ FISTA scheme

$\mathbf{z}_{j+1} = \mathbf{z}_j + \frac{t_j - 1}{t_{j+1}}(\mathbf{u}_j - \mathbf{u}_{j-1})$

▷ Update step $\mathcal{O}(NT)$

if $\|\mathbf{z}_{j+1} - \mathbf{z}_j\|_2^2 / (\|\mathbf{z}_j\|_2^2 + \delta) < \epsilon$ **then**

break

▷ Stopping criterion met

return \mathbf{z}_j

Before concluding, we remark that it is a simple corollary of Theorem 6 that when \mathbf{A} is jointly diagonalizable with \mathbf{L}_J , the problem is solved by a single joint filtering operation by the Wiener filter

$$g(\vartheta) = \frac{h_{\mathbf{x}}(\vartheta) a(\vartheta)}{a^2(\vartheta) h_{\mathbf{x}}(\vartheta) + h_{\mathbf{w}}(\vartheta)}, \quad (20)$$

the application of which, despite having the same asymptotic complexity, is much faster in practice.

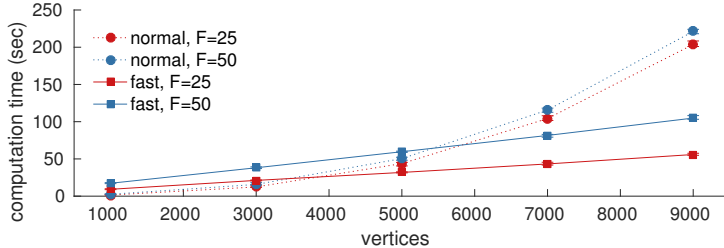


Figure 2: Scalability of the convolutional JPSD estimator. The fast implementation should be favored when the number graph is composed out of more than a few thousands vertices. The approximation error inherent in the fast implementation was negligible in our experiments.

6 Experiments

6.1 Joint Power Spectral Density Estimation

The first step in our evaluation is to analyze the efficiency of JPSD estimation. Our objective is dual. First, we aim to study the role of the different method parameters into the estimation accuracy and computational complexity, essentially providing practical guidelines for their usage. In addition, we wish to illustrate the usefulness of the joint stationarity assumption in learning from few samples.

Variance-bias-complexity tradeoffs. To validate the analysis of Section 4 for the computational and accuracy trade-offs inherent to our JPSD estimation method, we performed numerical experiments with synthetic graphs ($N = 256$ vertices and average degree slightly above 7) and JWSS processes ($T = 128$ timesteps). For simplicity, we focus on the standard setting of a Gaussian process with smooth and separable JPSD that is exponentially decreasing with frequency

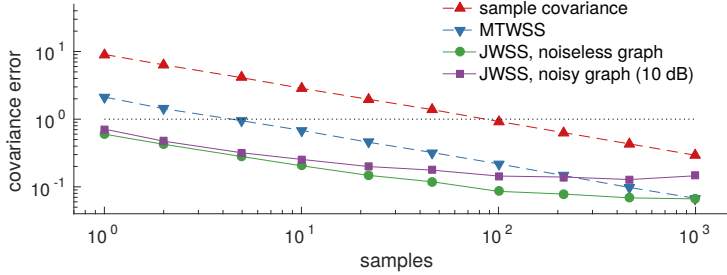
$$h(\vartheta) = e^{-\lambda/\lambda_{max}} e^{-5\omega^2}. \quad (21)$$

In our experience, similar JPSD are commonly found in data with smooth spatio-temporal structure, such as for instance in meteorological datasets. We remark that the presented results were found consistent with those obtained for non-separable JPSD and non-normal distributions. In this section, we examine the relation between the real JPSD $h(\Theta)$ and the convolutional estimate $\hat{h}(\Theta)$. Our metrics of error, bias, and variance (see caption of Figure 1) were estimated by a sample average of 20 experiments.

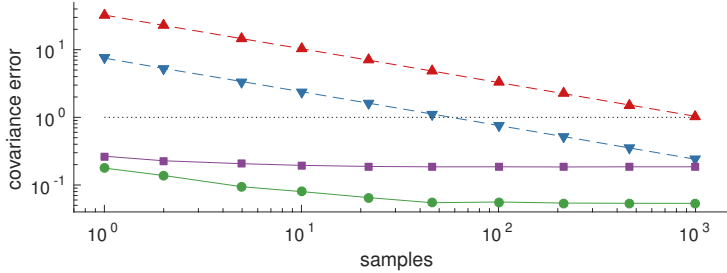
We remind the reader that there are two parameters influencing the performance of the proposed estimator: the window size L corresponding to our assumption for the support length of the autocorrelation in time, and the number of graph filters F used to capture power density in the graph spectral dimension. Figures 1 (a-d) report four key metrics for an exhaustive search of L, F combinations. We observe that large values of F and L generally improve the normalized RMSE (Figure 1a) because they result in reduced bias (Figure 1b). Nevertheless, setting the parameters to their maximum values is not suggested as the variance is increased (Figure 1c). In Figure 1d we see that, utilizing a large number of filters and number of windows (i.e., large F and small L), increases the average execution time.

Figure 2 delves further into the issue of scalability. In particular, we examine the min/median/max execution time of the convolutional JPSD estimator for increasing problem sizes when run in a desktop computer. Though the setting is identical to the previous experiments, here the number of vertices is varied from 1000 to 9000. We compare two implementations. The first, which naively performs the convolution in the spectral domain, uses the eigenvalue decomposition and therefore scales quadratically with the number of vertices. Due to its optimized code and simplicity, this should be the method of choice when N is small. For larger problems, we suggest using the fast implementation. As shown in the figure, this implementation scales linearly with N (here $E = \mathcal{O}(N)$) when the number of filters F and timesteps T are held constant.

How to choose L and F ? Having no computational constrains, one should choose the parameter combination that minimized the Akaike information criterion (AIC) score. This procedure is often infeasible as it is based on computing each model’s log-likelihood and thus entails estimating one JPSD for each parameterization in consideration. We have found experimentally that setting $F = \min(N, 50)$ provides a good trade-off between computational complexity and error. On the other hand, we suggest setting L equal to an upper bound of the autocorrelation support.



(a) $N = 10, T = 10$



(b) $N = 100, T = 10$

Figure 3: Even an approximate knowledge of the graph enables us to make good estimates of the covariance (and PSD) from very few samples. The joint stationarity prior becomes especially meaningful when the number of variables (N, T) increases.

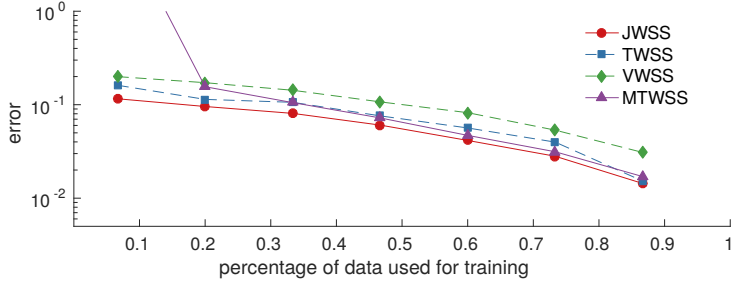
Learning from few samples. Figure 3 illustrates the benefit of a joint stationarity prior as compared to (i) a sample covariance estimator which makes no assumptions about the data, and (ii) the multivariate TWSS process estimator with optimal bandwidth [16]. As expected, an accurate estimation is challenging when the number of samples is much smaller than the number of problem variables (NT) , returning errors above one for the sample estimator. Introducing stationarity priors regularizes the estimation resulting in more stable estimates.

What is perhaps surprising is that, even when the graph (and \mathbf{U}_G) are known only approximately, estimating the second order moment of the distribution using the joint stationarity assumption is beneficial. To portray this phenomenon, we also plot the estimation error when using a noisy graph (we corrupted the weighted adjacency matrix by Gaussian noise, with SNR = 10 dB). Undoubtedly, introducing noise to the graph edges negatively affects estimation by introducing bias. Still, even with noise the proposed method significantly outperforms purely time-based methods when less than NT samples are available.

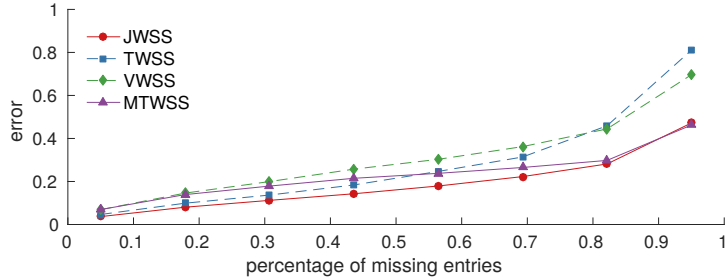
6.2 Recovery Performance on Three Datasets

We apply our methods on three diverse datasets featuring multivariate processes evolving over graphs: (a) a weather dataset depicting the temperature of 32 weather stations over one month, (b) a traffic dataset depicting high resolution daily vehicle flow of 4 weekdays, and (c) SIRS-type epidemics in Europe. Our experiments aim to show that joint stationarity is a useful model, even in datasets which may violate the strict conditions of our definition, and that -especially when few samples are available- it can yield a significant improvement in recovery performance, as compared to time- or vertex-based methods, on real datasets.

Experimental setup. We split the K samples of each dataset into a *training set* of size $p_t K$ and a *test set* of size $(1 - p_t)K$, respectively. After estimating the JPSD from the test set, we attempt to recover the values of $p_d NT$ variables randomly discarded from the test set. In each case, we report the RMSE for the recovered signal normalized by the ℓ_2 -norm of the original signal. We compare our joint method to the state-of-the-art wiener filters assuming *univariate time/vertex stationarity* [13]. Univariate stationarity methods solve the statistical recovery problem under the assumption that signals at stationary in the time/vertex domains, but considering different vertices/timesteps as independent. These methods are



(a) Influence of the training set size ($p = 30\%$)



(b) Influence of the percentage of missing values ($\rho = 20\%$)

Figure 4: Experiments with weather data. The joint approach becomes especially meaningful when the available data are few.

known to outperform non-model based methods, such as Tikhonov regularization (ridge regression) and total-variation regularization (lasso) over the time or graph dimensions [8, 9]. We also compare to the more involved *multivariate TWSS model* where the values at different vertices are correlated and the covariance is block Toeplitz of size $NT \times NT$. The latter is only shown for the weather dataset as the large number of variables present in the other datasets prohibited computation.

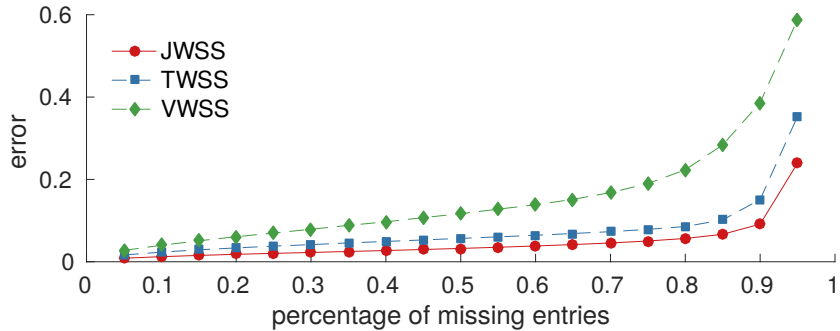
Molene dataset. The French national meteorological service has published in open access a dataset³ with hourly weather observations collected during the Month of January 2014 in the region of Brest (France). The graph is built from the coordinates of the weather stations by connecting all the neighbors in a given radius with a weight function $[W_G]_{i_1, i_2} = \exp(-k d(i_1, i_2)^2)$, where $d(i_1, i_2)$ is the euclidean distance between the stations i_1 and i_2 . Parameter k is adjusted to as obtain an average degree around 5 (k however is not a sensitive parameter). We split the data in $K = 15$ consecutive periods of $T = 48$ hours each. As sole pre-processing, we removed the mean (over time and stations) of the temperature.

We first test the influence of training set size p_t , while discarding $p_d = 30\%$ of the test variables. As seen in Figure 4a, the multivariate TWSS approach provides good recovery estimates when the when the number of samples is large, approaching that of joint stationarity, but suffers for small training sets (though not shown in the figure, the mean error was 9.8 when only $p_t = 10\%$ of the data was used for training). Due to their stricter modeling assumptions, disjoint stationarity methods returned relevant estimates when trained from very few samples, but exhibited larger bias. Figure 4b reports the achieved errors for recovery problems with progressively larger percentage $5\% \leq p_d \leq 95\%$ of discarded entries for a training percentage of $p_t = 20\%$. We can observe that the error trends are consistent across all cases.

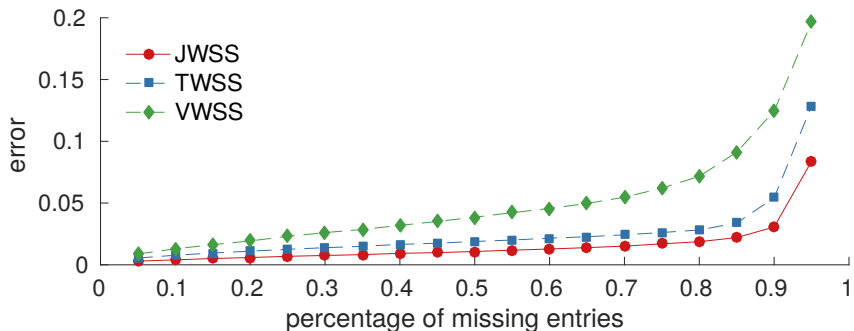
Traffic dataset. The California department of transportation publishes high-resolution traffic flow measurements (number of vehicles per unit interval) from stations deployed in the highways of Sacramento⁴. We focused at 727 stations over four weekdays in the period 01-06 April 2016. Starting from the road connectivity network obtained by the OpenStreetMap.org, we constructed one timeseries for each highway segment by setting the flow over it to be a weighted average of all nearby stations, while abiding to traffic direction. This resulted in a graph of $N = 710$ vertices, and a total of $T = 24 \times 12$ measurements per day for $K = 4$ days.

³Access to the raw data is possible directly from https://donneespubliques.meteofrance.fr/donnees_libres/Hackathon/RADOMEH.tar.gz

⁴The data correspond to the 3rd district of California and can be downloaded from <http://pems.dot.ca.gov/>



(a) 1 out of 4 days used for training ($\rho = 25\%$)



(b) 3 out of 4 days used for training ($\rho = 75\%$)

Figure 5: Experiments on Sacramento highway flow. By exploiting both graph and temporal dimensions, the joint approach closely captures the subtle variations in traffic throughout each weekday.

Figures 5a and 5b depict the mean recovery errors when the training sets were 1 and 3 days respectively. The strong temporal correlations present in highway traffic were useful in recovering missing values. Considering both the temporal and spatial dimension of the problem, resulted in very accurate estimates, with less than 0.04 error when $p = 50\%$ of the data were removed and the PSD was estimated from one day.

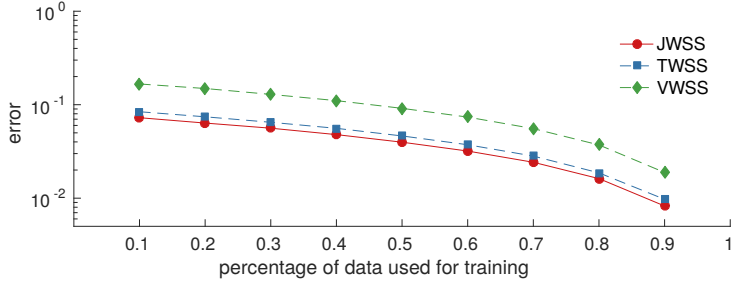
SIRS epidemic. Our third dataset depicts the spread of an infectious disease over $N = 200$ major cities of Europe, as predicted by the Susceptible-Infected-Recovered-Susceptible (SIRS) model, one of the standard models used to study epidemics. Our intention is to examine the predictive power of the considered methods when dealing with different realizations of a non-linear and probabilistic process over a graph (the data are fictitious). We parameterized SIRS as follows: length of infection period: 2 days, length of immunity period: 10 days, probability of contagion across neighboring cities per day: 0.005, total period: $T = 180$ days. We generated a total of $K = 10$ infections, all having the same starting point. As shown in Figures 6a and 6b, the attained results were consistent with the weather and traffic datasets.

We remark that our simulations were done using the GSPBOX [39], the UNLocBoX [40], and the LTFAT [41]. The code reproducing all figures will be made available soon.

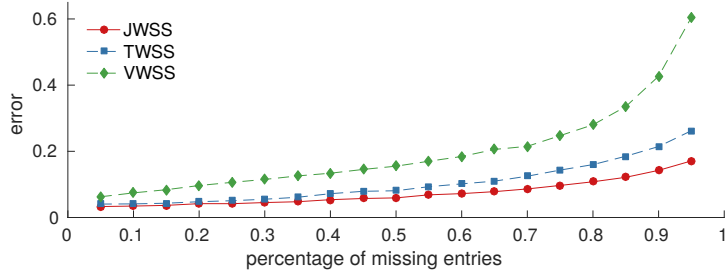
7 Conclusion

This paper proposed a novel definition of wide-sense stationarity appropriate for multivariate processes supported on the vertices of a graph. We showed that JWSS processes possess a number of familiar properties: (a) they are invariant to translation in the time-domain, (b) they can be generated by filtering noise, (c) and a joint Fourier transform diagonalizes their covariance.

Our model presents two key benefits. *First, the estimation and recovery of JWSS processes is very efficient, both in terms of sample and computational complexity.* In particular, the JPSD of a JWSS process can be estimated from very few (constant) number of samples at a complexity that is roughly linear to the number of graph edges and timesteps. After the PSD has been estimated, the linear MMSE recovery



(a) Influence of the training set size ($p = 30\%$)



(b) Influence of the percentage of missing entries ($\rho = 90\%$)

Figure 6: Experiments with the SIRS epidemic model.

problems of interpolation, denoising, and forecasting can be solved in the same asymptotic complexity. *Second, joint stationarity is a volatile model, able to capture non-trivial statistical relations in the temporal and vertex domains.* Our experiments suggested that we can model real spatio-temporal processes as jointly stationary without significant loss. Specifically, the JWSS prior was found more expressive than (univariate) TWSS and VWSS priors, and improved upon the multivariate time stationarity prior when the dimensionality was large but the samples few.

Acknowledgment

This work has been supported by the Swiss National Science Foundation research project *Towards Signal Processing on Graphs* (grant number: 2000_21/154350/1).

.1 Deferred proofs

Theorem 1. *If a process \mathbf{X} satisfies statement a, b or c in Definition 1, then it satisfies all of them.*

Proof. Before presenting the proof, we recall the following relation

$$\begin{aligned} h(\mathbf{L}_J)_{(i_1, t_1)(i_2, t_2)} &= \frac{1}{T} \sum_{n, \tau} h(\vartheta_{n, \tau}) \mathbf{u}_n^*(i_1) \mathbf{u}_n(i_2) e^{2\pi j \frac{(\tau-1)(t_2-t_1)}{T}} \\ &= \frac{1}{T} \sum_{\tau=1}^T [h_{\omega_\tau}(\mathbf{L}_G)]_{i_1, i_2} e^{2\pi j \frac{(\tau-1)(t_2-t_1)}{T}}, \end{aligned} \quad (22)$$

where $h_\omega(\lambda) = h(\lambda, \omega)$ and by abuse of notation, the indices $(i_1, t_1)(i_2, t_2)$ refer to the element at the $(t_1 - 1)N + i_1$ row and $(t_1 - 2)N + i_2$ column of the matrix. To prove an equivalence relation between the three statements, we will show $(a) \iff (c) \implies (b) \implies (a)$.

$(a) \iff (c)$. From the process described in (a), we can compute the mean as $\mathbf{E}[\mathbf{x}] = h(\mathbf{L}_J)\mathbf{c}$ and the covariance matrix as $\mathbf{E}[\mathbf{x}\mathbf{x}^*] - \bar{\mathbf{x}}\bar{\mathbf{x}}^* = h(\mathbf{L}_J)$. Since the \mathbf{c} is a vector that is in the null space of the graph Laplacian, it will stay in this space after filtering $\mathbf{L}_J\mathbf{E}[\mathbf{x}] = \mathbf{0}_{NT}$. The converse is trivial. For the

second moment, we start from (c). For $\tau = t_2 - t_1$, we have

$$\begin{aligned}\Gamma(t_1, t_2) &= \gamma_{t_2-t_1}(\mathbf{L}_G) \\ &= \frac{1}{T} \sum_{k=1}^T h_{w_k}(\mathbf{L}_G) e^{2\pi j \omega_k (t_2-t_1)}\end{aligned}\quad (23)$$

$$= h(\mathbf{L}_J)_{(\cdot, t_1)(\cdot, t_2)} \quad (24)$$

where (24) follows from (23) with $h_w(\lambda) = h(\lambda, \omega)$ and the last step is a consequence of (22). Therefore, the joint covariance matrix is the linear operator of the joint filter $h(\mathbf{L}_J)$. The converse is shown using the steps in reverse.

(c) \implies (b). From (c) and (24), it follows that $\Sigma_{\mathbf{x}} = h(\mathbf{L}_J) = \mathbf{U}_J h(\vartheta) \mathbf{U}_J^*$ implying $\Sigma_{\hat{\mathbf{x}}} = h(\vartheta)$ which is a diagonal matrix. As a result, the variables are uncorrelated. Additionally, since the mean is assumed in the null space of \mathbf{L}_J , all variables have mean 0 except for the DC component.

(b) \implies (a). From (b) we can model the variables in the spectral domain as: $\hat{\mathbf{x}} \sim \mathcal{D}(cNT\delta, h\vartheta)$, where $h(\vartheta) \succeq 0$. This implies that in the vertex domain, the process satisfies $\mathbf{x} \sim \mathcal{D}(\mathbf{c}, h(\mathbf{L}_J))$ where $\mathbf{L}_J \mathbf{c} = \mathbf{0}_{NT}$. Let us define the filter $h^{\frac{1}{2}}$ and the random variable $\boldsymbol{\varepsilon} \sim \mathcal{D}(c\mathbf{1}_{NT}, \mathbf{I}_{NT})$. We observe that filtering $\boldsymbol{\varepsilon}$ with $h^{\frac{1}{2}}$ leads to a process with the same statistics as the original process. \square

Theorem 2. *A joint process \mathbf{X} is JWSS if and only if it is both MTWSS and MVWSS.*

Proof. For the first movement, since $\mathbf{U}_J = \mathbf{U}_G \times \mathbf{U}_T$, it is straightforward to see that $\mathbf{L}_J \bar{\mathbf{x}} = \mathbf{0}_{NT}$ if and only if both $\mathbf{L}_G \bar{\mathbf{x}}_t = \mathbf{0}_N$ and $\mathbf{L}_T \bar{\mathbf{x}}^i = \mathbf{0}_T$, hold for all t and i . Furthermore since the eigenvector associated to the null space of \mathbf{L}_T is constant, the condition $\mathbf{L}_T \bar{\mathbf{x}}^i = \mathbf{0}_T$ implies that $\bar{\mathbf{X}}_{i,t} = c_i$.

For the second moment, we observe that $\Gamma(t_1, t_2) = \gamma_\tau(\mathbf{L}_G)$ with $\tau = t_2 - t_1$ if and only if $\Gamma(t_1, t_2) = \Gamma(\tau)$ and $\Gamma(t_1, t_2) = \Gamma_{t_2-t_1}(\mathbf{L}_G)$. \square

Property 3. *When a joint filter $f(\mathbf{L}_J)$ is applied to a JWSS process \mathbf{X} , the result \mathbf{Y} remains JWSS with mean $f(0, 0)\mathbf{E}[\mathbf{X}]$ and JPSD $f^2(\vartheta_{n,\tau}) h_{\mathbf{x}}(\vartheta_{n,\tau})$.*

Proof. The output of a filter $f(\mathbf{L}_J)$ can be written in vector form as $\mathbf{y} = f(\mathbf{L}_J)\mathbf{x}$. If the input signal \mathbf{x} is JWSS, we can confirm that the first moment of the filter output is zero, $f(\mathbf{L}_J)\bar{\mathbf{x}} = f(0, 0)\mathbf{E}[\mathbf{x}]$. The last equality follows from the fact that by definition $\mathbf{E}[\mathbf{x}]$ is in the null space of \mathbf{L}_J . The computation of the second moment gives

$$\begin{aligned}\Sigma_{\mathbf{y}} &= \mathbf{E}[f(\mathbf{L}_J)\mathbf{x} (f(\mathbf{L}_J)\mathbf{x})^*] - \mathbf{E}[h(\mathbf{L}_J)\mathbf{x}] \mathbf{E}[(f(\mathbf{L}_J)\mathbf{x})^*] \\ &= f(\mathbf{L}_J)\mathbf{E}[\mathbf{x}\mathbf{x}^*] f(\mathbf{L}_J) - f(\mathbf{L}_J)\bar{\mathbf{x}}\bar{\mathbf{x}}^* f(\mathbf{L}_J)^* \\ &= f(\mathbf{L}_J)\Sigma_{\mathbf{x}} f(\mathbf{L}_J)^* \\ &= \mathbf{U}_J (f^2(\vartheta) h_{\mathbf{x}}(\vartheta)) \mathbf{U}_J^*,\end{aligned}$$

which is JWSS as it is diagonalizable by \mathbf{U}_J (Theorem 1). \square

Lemma 1. *If function $h(\vartheta)$ is ϵ -Lipschitz, then the bias is bounded by*

$$\left| \mathbf{E}[\ddot{h}(\vartheta) - h(\vartheta)] \right| \leq \frac{\epsilon}{c_g(\vartheta)} \sum_{n=1, \tau=1}^{T, N} g(\vartheta - \vartheta_{n,\tau})^2 \|\vartheta - \vartheta_{n,\tau}\|_2.$$

Proof. Using the Lipschitz property of $h(\vartheta)$, we write

$$\begin{aligned}\left| \mathbf{E}[\ddot{h}(\vartheta) - h(\vartheta)] \right| &= \left| \sum_{n,\tau=1}^{NT} g(\vartheta - \vartheta_{n,\tau})^2 \frac{h(\vartheta_{n,\tau})}{c_g(\vartheta)} - h(\vartheta) \right| \\ &\leq |A h(\vartheta)| + \frac{\epsilon}{c_g(\vartheta)} \sum_{n,\tau=1}^{NT} g(\vartheta - \vartheta_{n,\tau})^2 \|\vartheta - \vartheta_{n,\tau}\|\end{aligned}$$

where by definition $A = \sum_{k=1}^{NT} \frac{g^2(\vartheta - \vartheta_{n,\tau})}{c_g(\vartheta)} - 1 = 0$, and the claim follows. \square

Lemma 2. For any distribution with bounded second and fourth order moments, the convolutional estimate has variance

$$\text{Var} [\ddot{h}(\vartheta)] = \sum_{n,\tau}^{N,T} \frac{g(\vartheta - \vartheta_{n,\tau})^4}{c_g(\vartheta)^2} h(\vartheta_{n,\tau})^2 \frac{\mathbf{E}[\hat{\varepsilon}_{n,\tau}^4] - 1}{K}. \quad (25)$$

Proof. Set $w_{n,\tau} = \frac{g(\vartheta - \vartheta_{n,\tau})^2}{c_g(\vartheta)}$. The centered random variable

$$\ddot{h}(\vartheta) - h(\vartheta) = \sum_{n,\tau}^{N,T} w_{n,\tau} (\dot{h}(\vartheta_{n,\tau}) - h(\vartheta_{n,\tau}))$$

is a weighted sum of independent random variables $\dot{h}(\vartheta_{n,\tau}) - h(\vartheta_{n,\tau})$, which according to Theorem 3 have variance $h^2(\vartheta_{n,\tau}) \frac{\mathbf{E}[\hat{\varepsilon}_{n,\tau}^4] - 1}{K}$. It follows that,

$$\begin{aligned} \text{Var} [\ddot{h}(\vartheta)] &= \sum_{n,\tau}^{N,T} w_{n,\tau}^2 \mathbf{E} [(\dot{h}(\vartheta_{n,\tau}) - h(\vartheta_{n,\tau}))^2] \\ &= \sum_{n,\tau}^{N,T} w_{n,\tau}^2 h^2(\vartheta_{n,\tau}) \frac{\mathbf{E}[\hat{\varepsilon}_{n,\tau}^4] - 1}{K}, \end{aligned}$$

which matches our claim. \square

Theorem 5. If \mathbf{x} is JWSS with PSD $h_{\mathbf{x}}(\mathbf{L}_J)$ and \mathbf{w} is i.i.d white noise with $h_{\mathbf{w}}(\mathbf{L}_J) = \sigma^2 \mathbf{I}$, then the solutions of Problems (P1) and (P2) are linear minimum mean squared estimators.

Proof. We start with some basic facts. Under the linear measurement model, vector \mathbf{y} has mean $\bar{\mathbf{y}} = \mathbf{A}\bar{\mathbf{x}}$ and covariance $\Sigma_{\mathbf{y}} = \mathbf{B}\mathbf{B}^* + \sigma^2 \mathbf{I}$, where $\mathbf{B} = \mathbf{A}h_{\mathbf{x}}(\mathbf{L}_J)^{1/2}$. The covariance between \mathbf{x} and \mathbf{y} is $\Sigma_{\mathbf{xy}} = \Sigma_{\mathbf{yx}}^* = h_{\mathbf{x}}(\mathbf{L}_J)\mathbf{A}^*$. Moreover, for simplicity, let $h_{\mathbf{x}}(\mathbf{L}_J)$ and $\Sigma_{\mathbf{y}}$ be invertible, however this assumption is not necessary. After the change of variables $\tilde{\mathbf{x}} = \mathbf{x} - \bar{\mathbf{x}}$, $\tilde{\mathbf{y}} = \mathbf{y} - \bar{\mathbf{y}}$, (P1) reads,

$$\hat{\tilde{\mathbf{x}}} = \arg \min_{\tilde{\mathbf{x}}} \|\mathbf{A}\tilde{\mathbf{x}} - \tilde{\mathbf{y}}\|_2^2 + \sigma^2 \|h_{\mathbf{x}}^{-\frac{1}{2}}(\mathbf{L}_J)\tilde{\mathbf{x}}\|_2^2, \quad (26)$$

which has the closed-form solution

$$\begin{aligned} \hat{\tilde{\mathbf{x}}} &= (\mathbf{A}^* \mathbf{A} + \sigma^2 h_{\mathbf{x}}^{-1}(\mathbf{L}_J))^{-1} \mathbf{A}^* \tilde{\mathbf{y}} \\ &= h_{\tilde{\mathbf{x}}}^{\frac{1}{2}}(\mathbf{L}_J) (\sigma^2 \mathbf{I} + \mathbf{B}^* \mathbf{B})^{-1} \mathbf{B}^* \tilde{\mathbf{y}} \end{aligned}$$

From the Woodbury, Sherman, and Morrison matrix identity

$$\begin{aligned} (\sigma^2 \mathbf{I} + \mathbf{B}^* \mathbf{B})^{-1} &= \sigma^{-2} - \sigma^{-2} \mathbf{B}^* (\mathbf{I} + \mathbf{B} \sigma^{-2} \mathbf{B}^*)^{-1} \mathbf{B} \sigma^{-2} \\ &= \sigma^{-2} (\mathbf{I} - \mathbf{B}^* (\sigma^2 \mathbf{I} + \mathbf{B}\mathbf{B}^*)^{-1} \mathbf{B}) \end{aligned}$$

and the expression for $\hat{\tilde{\mathbf{x}}}$ can be re-written as

$$\begin{aligned} \hat{\tilde{\mathbf{x}}} &= \sigma^{-2} h_{\mathbf{x}}(\mathbf{L}_J) \mathbf{A}^* \left(\mathbf{I} - (\sigma^2 \mathbf{I} + \mathbf{B}^* \mathbf{B})^{-1} \mathbf{B}\mathbf{B}^* \right) \tilde{\mathbf{y}} \\ &= h_{\mathbf{x}}(\mathbf{L}_J) \mathbf{A}^* (\sigma^2 \mathbf{I} + \mathbf{B}^* \mathbf{B})^{-1} \tilde{\mathbf{y}} = \Sigma_{\mathbf{xy}} \Sigma_{\mathbf{y}}^{-1} \tilde{\mathbf{y}} \end{aligned}$$

where this time we used the reverse Woodbury identity. It follows that

$$\begin{aligned} \hat{\mathbf{x}} &= \hat{\tilde{\mathbf{x}}} + \bar{\mathbf{x}} \\ &= \Sigma_{\mathbf{xy}} \Sigma_{\mathbf{y}}^{-1} (\mathbf{y} - \mathbf{A}\bar{\mathbf{x}}) + \bar{\mathbf{x}} \\ &= \Sigma_{\mathbf{xy}} \Sigma_{\mathbf{y}}^{-1} \mathbf{y} + (\mathbf{I} - \Sigma_{\mathbf{xy}} \Sigma_{\mathbf{y}}^{-1} \mathbf{A}) \bar{\mathbf{x}} \\ &= \mathbf{Q}\mathbf{y} + (\mathbf{I} - \mathbf{Q}\mathbf{A}) \bar{\mathbf{x}}, \end{aligned}$$

which is equivalent to the linear minimum mean square error estimator $\hat{\mathbf{x}} = \arg \min_{\mathbf{Q}, \mathbf{b}} \mathbf{E} [\|(\mathbf{Q}\mathbf{y} + \mathbf{b}) - \hat{\mathbf{x}}\|_2^2]$ with $\mathbf{y} = \mathbf{A}\mathbf{x} + \mathbf{w}$. See [42, Equation 12.6].

Using similar arguments, one derives that the solution of Problem (P2) is

$$\hat{\mathbf{x}} = h_{\mathbf{x}}(\mathbf{L}_J) (\mathbf{B}\mathbf{B}^*)^{-1} \mathbf{y} + \left(\mathbf{I} - h_{\mathbf{x}}(\mathbf{L}_J) (\mathbf{B}\mathbf{B}^*)^{-1} \mathbf{A} \right) \bar{\mathbf{x}}$$

and is thus a linear minimum mean square estimator too. \square

Theorem 6. *If the operator \mathbf{A} is jointly diagonalizable with \mathbf{L}_J , such that $\mathbf{A} = a(\mathbf{L}_J)$, then the solutions of Problems (P1) and (P2) match that of (P0).*

Proof. The following is a generalization of the classical proof. For simplicity, we assume that $\mathbf{E}[\mathbf{L}_J \mathbf{x}] = 0$. By hypothesis $\mathbf{A} = a(\mathbf{L}_J) = \mathbf{U}_J a(\mathbf{\Lambda}_J) \mathbf{U}_J^*$, we can rewrite the optimization problem (P1) in the joint spectral domain using the Parseval identity $\|\mathbf{x}\|_2 = \|\mathbf{U}_J^* \mathbf{x}\|_2 = \|\hat{\mathbf{x}}\|_2$:

$$\hat{\mathbf{x}} = \arg \min_{\hat{\mathbf{x}}} \|f(\mathbf{\Lambda}_J) \hat{\mathbf{x}}\|_2^2 + \|a(\mathbf{\Lambda}_J) \hat{\mathbf{x}} - \hat{\mathbf{y}}\|_2^2.$$

Since the matrix $a(\mathbf{\Lambda}_J)$ is diagonal, the solution of this problem satisfies for pairs of graph eigenvalue, frequency $\vartheta_{n\tau} = [\lambda_n, \omega_\tau]$.

$$\begin{aligned} f^2(\vartheta_{n\tau}) \hat{\mathbf{x}}(\vartheta_{n\tau}) + h^2(\vartheta_{n\tau}) \hat{\mathbf{x}}(\vartheta_{n\tau}) \\ = h(\vartheta_{n\tau}) \hat{\mathbf{y}}(\vartheta_{n\tau}). \end{aligned} \quad (27)$$

The previous equation is transformed in

$$\hat{\mathbf{x}} = \frac{h(\vartheta_{n\tau})}{f^2(\vartheta_{n\tau}) + a^2(\vartheta_{n\tau})} \hat{\mathbf{y}}.$$

As a next step, we use the fact that $\hat{\mathbf{y}} = a(\vartheta_{n\tau}) \hat{\mathbf{x}} + \hat{\mathbf{w}}$ to find

$$\hat{\mathbf{x}} = \frac{a^2(\vartheta_{n\tau}) \hat{\mathbf{x}} + a(\vartheta_{n\tau}) \hat{\mathbf{w}}}{f^2(\vartheta_{n\tau}) + a^2(\vartheta_{n\tau})}.$$

The recovery error is

$$\hat{\mathbf{e}} = \hat{\mathbf{x}} - \hat{\mathbf{x}} = \frac{-f^2(\vartheta_{n\tau}) \hat{\mathbf{x}}}{f^2(\vartheta_{n\tau}) + a^2(\vartheta_{n\tau})} + \frac{a(\vartheta_{n\tau}) \hat{\mathbf{w}}}{f^2(\vartheta_{n\tau}) + a^2(\vartheta_{n\tau})}.$$

For simplicity, we drop the notation $(\vartheta_{n\tau})$. We then have that

$$\begin{aligned} \mathbf{E}[\hat{\mathbf{e}}^2] &= \frac{f^4 \mathbf{E}[\hat{\mathbf{x}}^2] + a^2(\mathbf{E}[\hat{\mathbf{w}}^2] - f^2 \mathbf{E}[\hat{\mathbf{x}} \hat{\mathbf{w}}])}{(f^2 + a^2)^2} \\ &= \frac{f^4 h_{\mathbf{x}} + a^2 h_{\mathbf{w}}}{(f^2 + a^2)^2}, \end{aligned}$$

with $h_{\mathbf{x}}$ the PSD of \mathbf{x} and $h_{\mathbf{w}}$ the PSD of the noise \mathbf{w} . Note that $\mathbf{E}[\hat{\mathbf{x}} \hat{\mathbf{w}}] = 0$ because \mathbf{x} and \mathbf{w} are uncorrelated. Let us now substitute $f^2(\vartheta_{n\tau})$ by z and minimize the expected error (for each pair $\vartheta_{n\tau} = [\lambda_n, \omega_\tau]$) with respect to z .

$$\begin{aligned} \frac{\partial}{\partial z} \mathbf{E}[\hat{\mathbf{e}}^2] &= \frac{\partial}{\partial z} \frac{z^2 h_{\mathbf{x}} + a^2 h_{\mathbf{w}}}{(z + a^2)^2} \\ &= \frac{2z h_{\mathbf{x}} (z + a^2) - 2(z^2 h_{\mathbf{x}} + a^2 h_{\mathbf{w}})}{(z + a^2)^3} = 0. \end{aligned}$$

From the numerator, we get $2z h_{\mathbf{x}} a^2 - 2a^2 h_{\mathbf{w}} = 0$. The three possible solutions for z are $z_1 = \frac{h_{\mathbf{w}}}{h_{\mathbf{x}}}$, $z_2 = \infty$ and $z_3 = -\infty$. Solution z_3 is not possible because z is required to be positive. Solution z_2 leads to $\hat{\mathbf{x}} = 0$ which is optimal only if $h_{\mathbf{x}} = 0$. The optimal solution is therefore $z(\vartheta_{n\tau}) = \frac{h_{\mathbf{w}}(\vartheta_{n\tau})}{h_{\mathbf{x}}(\vartheta_{n\tau})}$, resulting in

$$f(\vartheta_{n\tau}) = \sqrt{\frac{h_{\mathbf{w}}(\vartheta_{n\tau})}{h_{\mathbf{x}}(\vartheta_{n\tau})}}.$$

This finishes the first part of the proof. To show that the solution of (P1) is a Wiener filtering operation, we replace $f^2(\vartheta_{n\tau})$ by $\frac{h_{\mathbf{w}}(\vartheta_{n\tau})}{h_{\mathbf{x}}(\vartheta_{n\tau})}$ in (27) and find

$$\hat{\mathbf{x}}(\vartheta_{n\tau}) = \frac{h_{\mathbf{x}}(\vartheta_{n\tau}) a(\vartheta_{n\tau})}{a^2(\vartheta_{n\tau}) h_{\mathbf{x}}(\vartheta_{n\tau}) + h_{\mathbf{w}}(\vartheta_{n\tau})} \hat{\mathbf{y}}(\vartheta_{n\tau}),$$

which is the Wiener filter associated with $a(\mathbf{L}_J) = \mathbf{A}$. \square

References

- [1] M. Rudelson, “Random vectors in the isotropic position,” *Journal of Functional Analysis*, vol. 164, no. 1, pp. 60–72, 1999.
- [2] M. J. Keeling and K. T. Eames, “Networks and epidemic models,” *Journal of the Royal Society Interface*, vol. 2, no. 4, pp. 295–307, 2005.
- [3] P. Mohan, V. N. Padmanabhan, and R. Ramjee, “Nericell: rich monitoring of road and traffic conditions using mobile smartphones,” in *Proceedings of the 6th ACM conference on Embedded network sensor systems*. ACM, 2008, pp. 323–336.
- [4] W. Huang, L. Goldsberry, N. F. Wymbs, S. T. Grafton, D. S. Bassett, and A. Ribeiro, “Graph frequency analysis of brain signals,” *arXiv preprint arXiv:1512.00037*, 2015.
- [5] F. Zhang and E. R. Hancock, “Graph spectral image smoothing using the heat kernel,” *Pattern Recognition*, vol. 41, no. 11, pp. 3328–3342, 2008.
- [6] A. J. Smola and R. Kondor, “Kernels and regularization on graphs,” in *Learning theory and kernel machines*. Springer, 2003, pp. 144–158.
- [7] M. Belkin and P. Niyogi, “Semi-supervised learning on riemannian manifolds,” *Machine learning*, vol. 56, no. 1-3, pp. 209–239, 2004.
- [8] D. I. Shuman, S. K. Narang, P. Frossard, A. Ortega, and P. Vandergheynst, “The emerging field of signal processing on graphs: Extending high-dimensional data analysis to networks and other irregular domains,” *Signal Processing Magazine, IEEE*, vol. 30, no. 3, pp. 83–98, 2013.
- [9] A. Sandryhaila and J. M. Moura, “Discrete signal processing on graphs,” *IEEE transactions on signal processing*, vol. 61, pp. 1644–1656, 2013.
- [10] A. Gadde and A. Ortega, “A probabilistic interpretation of sampling theory of graph signals,” *arXiv preprint arXiv:1503.06629*, 2015.
- [11] C. Zhang, D. Florêncio, and P. A. Chou, “Graph signal processing—a probabilistic framework,” *Microsoft Res., Redmond, WA, USA, Tech. Rep. MSR-TR-2015-31*, 2015.
- [12] A. Loukas and D. Foccard, “Frequency analysis of temporal graph signals,” *arXiv preprint arXiv:1602.04434*, 2016.
- [13] N. Perraudin and P. Vandergheynst, “Stationary signal processing on graphs,” *arXiv preprint arXiv:1601.02522*, 2016.
- [14] B. Girault, “Stationary graph signals using an isometric graph translation,” in *Signal Processing Conference (EUSIPCO), 2015 23rd European*. IEEE, 2015, pp. 1516–1520.
- [15] A. G. Marques, S. Segarra, G. Leus, and A. Ribeiro, “Stationary graph processes and spectral estimation,” *arXiv preprint arXiv:1603.04667*, 2016.
- [16] N. Wiener and P. Masani, “The prediction theory of multivariate stochastic processes,” *Acta Mathematica*, vol. 98, no. 1, pp. 111–150, 1957.
- [17] —, “The prediction theory of multivariate stochastic processes, ii,” *Acta Mathematica*, vol. 99, no. 1, pp. 93–137, 1958.
- [18] P. Bloomfield, *Fourier analysis of time series: an introduction*. John Wiley & Sons, 2004.
- [19] F. R. Bach and M. I. Jordan, “Learning graphical models for stationary time series,” *IEEE transactions on signal processing*, vol. 52, no. 8, pp. 2189–2199, 2004.
- [20] R. Dahlhaus and M. Eichler, “Causality and graphical models in time series analysis,” *Oxford Statistical Science Series*, pp. 115–137, 2003.
- [21] B. Girault, “Signal processing on graphs-contributions to an emerging field,” Ph.D. dissertation, Ecole normale supérieure de lyon, 2015.

- [22] S. P. Chepuri and G. Leus, “Subsampling for graph power spectrum estimation,” *arXiv preprint arXiv:1603.03697*, 2016.
- [23] A. Loukas and N. Perraudin, “Predicting the evolution of stationary graph signals,” *arXiv preprint arXiv:1607.03313*, 2016.
- [24] J. Mei and J. M. Moura, “Signal processing on graphs: Causal modeling of unstructured data,” *arXiv preprint arXiv:1503.00173*, 2015.
- [25] N. Perraudin, A. Loukas, F. Grassi, and P. Vandergheynst, “Towards stationary time-vertex signal processing,” *arXiv preprint arXiv:1606.06962*, 2016.
- [26] D. K. Hammond, P. Vandergheynst, and R. Gribonval, “Wavelets on graphs via spectral graph theory,” *Applied and Computational Harmonic Analysis*, vol. 30, no. 2, pp. 129–150, 2011.
- [27] D. I. Shuman, B. Ricaud, and P. Vandergheynst, “Vertex-frequency analysis on graphs,” *arXiv preprint arXiv:1307.5708*, 2013.
- [28] G. Strang, “The discrete cosine transform,” *SIAM review*, vol. 41, no. 1, pp. 135–147, 1999.
- [29] N. Perraudin, B. Ricaud, D. Shuman, and P. Vandergheynst, “Global and local uncertainty principles for signals on graphs,” *arXiv preprint arXiv:1603.03030*, 2016.
- [30] R. Vershynin, “How close is the sample covariance matrix to the actual covariance matrix?” *Journal of Theoretical Probability*, vol. 25, no. 3, pp. 655–686, 2012.
- [31] M. S. Bartlett, “Periodogram analysis and continuous spectra,” *Biometrika*, pp. 1–16, 1950.
- [32] P. Welch, “The use of fast fourier transform for the estimation of power spectra: a method based on time averaging over short, modified periodograms,” *IEEE Transactions on audio and electroacoustics*, pp. 70–73, 1967.
- [33] K. Gröchenig, *Foundations of time-frequency analysis*. Springer Science & Business Media, 2013.
- [34] H. G. Feichtinger and T. Strohmer, *Gabor analysis and algorithms: Theory and applications*. Springer Science & Business Media, 2012.
- [35] C. De Boor, C. De Boor, E.-U. Mathématicien, C. De Boor, and C. De Boor, *A practical guide to splines*. Springer-Verlag New York, 1978, vol. 27.
- [36] A. Susnjara, N. Perraudin, D. Kressner, and P. Vandergheynst, “Accelerated filtering on graphs using lanczos method,” *arXiv preprint arXiv:1509.04537*, 2015.
- [37] A. Beck and M. Teboulle, “A fast iterative shrinkage-thresholding algorithm for linear inverse problems,” *SIAM journal on imaging sciences*, vol. 2, no. 1, pp. 183–202, 2009.
- [38] P. L. Combettes and J.-C. Pesquet, “A douglas–rachford splitting approach to nonsmooth convex variational signal recovery,” *IEEE Journal of Selected Topics in Signal Processing*, vol. 1, no. 4, pp. 564–574, 2007.
- [39] N. Perraudin, J. Paratte, D. Shuman, V. Kalofolias, P. Vandergheynst, and D. K. Hammond, “GSP-BOX: A toolbox for signal processing on graphs,” *ArXiv e-prints*, Aug. 2014.
- [40] N. Perraudin, D. Shuman, G. Puy, and P. Vandergheynst, “UNLocBoX A matlab convex optimization toolbox using proximal splitting methods,” *ArXiv e-prints*, Feb. 2014.
- [41] in *Sound, Music, and Motion*, ser. Lecture Notes in Computer Science, 2014.
- [42] S. M. Kay, *Fundamentals of statistical signal processing: estimation theory*. Prentice-Hall, Inc., 1993.